Journal of Magnetism and Magnetic Materials 468 (2018) 273–278

Contents lists available at ScienceDirect

Journal of Magnetism and Magnetic Materials

journal homepage: www.elsevier.com/locate/jmmm

Research articles

Time domain magnetization dynamics study to estimate interlayer exchange coupling constant in Nd-Fe-B/$Ni_{80}Fe_{20}$ films

R. Mandal[a,*], D. Ogawa[a], Y. Tamazawa[c], K. Ishioka[b], T. Shima[c], T. Kato[d], S. Iwata[d], Y.K. Takahashi[a,*], S. Hirosawa[a], K. Hono[a]

[a] Research Center for Magnetic and Spintronic Materials, National Institute for Materials Science, 1-2-1 Sengen, Tsukuba 305-0047, Japan
[b] Research Center for Advanced Measurement and Characterization, National Institute for Materials Science, 1-2-1 Sengen, Tsukuba 305-0047, Japan
[c] Tohoku Gakuin University, 1-13-1, Chuo, Tagajo 986-8537, Japan
[d] Nagoya University, Furo-cho, Chikusa-ku, Nagoya 464-8603, Japan

A B S T R A C T

Interlayer exchange coupling (J_{ex}) between a hard magnetic Nd-Fe-B layer and a soft magnetic $Ni_{80}Fe_{20}$ layer is studied by means of time-resolved magneto-optical Kerr effect (TRMOKE) microscope. Whereas a single 16 nm thick Nd-Fe-B layer without $Ni_{80}Fe_{20}$ showed high coercivity of $\mu_0 H_c = 2$ T and resonance frequency of $f_r = 161$ GHz at external bias magnetic field of $\mu_0 H_b = 2$ T due to the high anisotropy field, those of the bi-layer Nd-Fe-B (16 nm)/$Ni_{80}Fe_{20}$ (5 nm) are dramatically reduced to $\mu_0 H_c = 1.34$ T and $f_r = 74.4$ GHz. When the Nd-Fe-B and $Ni_{80}Fe_{20}$ are separated by a 1 nm thick non-magnetic Mo layer, by contrast, the coercivity recovered partially to $\mu_0 H_c = 1.9$ T but the frequency further reduced to $f_r = 63.4$ GHz. We derived J_{ex} based on a simple macrospin model, whose value reduced from 3.9 ± 0.1 mJ/m^2 for the bi-layer without the Mo layer to 0.1 ± 0.1 mJ/m^2 with the Mo layer. The reduction in J_{ex} suggested that the interlayer exchange decoupling between the Nd-Fe-B and the $Ni_{80}Fe_{20}$ layers was responsible to the recovery of $\mu_0 H_c$ and the reduction of f_r by the insertion of the non-magnetic layer. We successfully estimated the interlayer exchange coupling constant in the hard/soft magnetic bilayer system by TRMOKE and macrospin-modeling, which had been previously difficult because of its high anisotropy and high coercivity. This method is applicable also to the quantitative estimation of the intergranular exchange coupling.

1. Introduction

Development of high-performance permanent magnet with large energy product, $(BH)_{max}$ has gained intense research interest in the permanent magnet community due to the wide range of applications in the energy saving traction motors of hybrid and pure electric vehicles and also in wind power generators. $(BH)_{max}$ is solely depends on coercivity ($\mu_0 H_c$), remanence magnetization (B_r) and squareness of magnets. Exchange spring magnets [1,2], containing hard and soft magnetic phases that are coupled with each other by strong exchange interaction through the interface, have been found to be a potential candidate for high-performance magnets [3] with substantially enhanced $(BH)_{max}$. The hard magnetic phase provides high anisotropy and coercive field whereas the soft magnetic phase is liable for enhanced magnetic moment [4]. Additionally, soft magnetic phase reduces rare-earth content and also acts as a protective layer for hard magnetic layer against corrosion. After the prediction of giant $(BH)_{max}$ value [3], the exchange-coupled behavior in $Sm_{20}Co_{80}/Fe_{65}Co_{35}$ bilayer film [5] and the remanence-enhanced behavior for Nd-Fe-B/Fe/Nd-Fe-B trilayer film [6] was reported. Recent progress of thin-film deposition technique shows a path to achieve high $(BH)_{max}$ value. Zhang et al. reported the $(BH)_{max}$ of 255 kJ/m^3 for $Sm(Co\text{-}Cu)_5$/Fe film system [7]. This experimental value is much larger than that of commercially available bulk $SmCo_5$ sintered magnet. Theoretical calculation predicted that Nd-Fe-B based nanocomposite magnet such as anisotropic $Nd_2Fe_{14}B/\alpha$-Fe system should possess $(BH)_{max}$ value of 700 kJ/m^3 [8]. However, the experimentally reported value is still much smaller than the predicted value [9,10]. The gap between this theoretical and experimental value is due to the difficulty in obtaining high coercivity in hard/soft exchange magnets, precise control over the grain size, its distribution and alignment of the hard-phase grains. Control over the microstructure results in the modification of exchange coupling through the interface. The exchange coupling is a key factor for determining the magnetic properties such as coercivity and remanent magnetization. To control the exchange coupling between hard and soft phases, insertion of a very thin non-magnetic spacer layer between them is helpful. For example, Cui et al. reported the recovery of $\mu_0 H_c$ and B_r by the insertion of Ta between Nd-Fe-B and Fe layers [11–14].

Although the control of the exchange coupling between soft and hard layers is the key for obtaining high $\mu_0 H_c$ and B_r, the quantification

* Corresponding authors at: Research Center for Magnetic and Spintronic Materials, National Institute for Materials Science, 1-2-1 Sengen, Tsukuba 305-0047, Japan.
E-mail addresses: mandal.ruma@nims.go.jp (R. Mandal), takahashi.yukiko@nims.go.jp (Y.K. Takahashi).

https://doi.org/10.1016/j.jmmm.2018.08.010
Received 3 May 2018; Received in revised form 23 July 2018; Accepted 5 August 2018
Available online 06 August 2018
0304-8853/

of the exchange coupling in the $Nd_2Fe_{14}B$ system is difficult because of its high magneto-crystalline anisotropy (K_u). Recently few reports [15–17] on the exchange coupling between $Nd_2Fe_{14}B$ and α-Fe in the thick nanocomposite magnet using ferromagnetic resonance (FMR) with high magnetic field and high frequency were reported. They found that the strong absorptions originating from the Fe and $Nd_2Fe_{14}B$ layer and the resonance magnetic field gets shifted depending on the volume fraction of α-Fe. Since the conventional FMR system has limited magnetic field and frequency, it is difficult to obtain the absorption signal from very high K_u materials because the FMR frequency is proportional to the effective magnetic field in the materials. One of the powerful tools for estimating the exchange coupling from the resonance frequency is time-resolved magneto-optical Kerr effect (TRMOKE), since it can divide pico-second time range which corresponds to the frequency of THz. There were few reports on the exchange coupling in the exchange-spring bi-layer system [18,19] using TRMOKE. However, there is no report on the estimation of the exchange coupling in the hard Nd-Fe-B magnetic thin film because of the difficulty in the observation of the spin precession which may be due to small amplitude of spin precession.

Here, we present a systematic study of the interlayer exchange coupling and ultrafast precessional magnetization dynamics of Nd-Fe-B (16 nm)/Mo (d_{Mo} nm)/$Ni_{80}Fe_{20}$ (5 nm) multilayer film with varying thickness d_{Mo}. We choose Nd-Fe-B as a hard magnetic layer and $Ni_{80}Fe_{20}$ as a soft magnetic layer. Although the magnetization of $Ni_{80}Fe_{20}$ is lower than Fe, we use it as soft magnetic material because the magnetization precession can be easily introduced. We have observed that the presence of spacer Mo layer significantly modifies the magnetic properties such as coercivity, demagnetization behavior of the film and also the precessional magnetization dynamics is strongly dominated by high anisotropy field of the hard magnetic layer as well as by the interlayer exchange coupling. We have employed a simple numerical modeling based on a macrospin approximation to evaluate the interlayer exchange coupling constant.

2. Experimental details

Nd-Fe-B/Mo (d_{Mo} nm)/$Ni_{80}Fe_{20}$ multilayer thin films were deposited on single crystalline MgO (1 0 0) substrate using an ultra-high vacuum magnetron sputtering system with a base pressure of 4×10^{-7} Pa. The film had the stacking structure of MgO (1 0 0) sub./Mo (20 nm)/Nd-Fe-B (16 nm)/Mo (d_{Mo} nm)/$Ni_{80}Fe_{20}$ (5 nm)/SiN (30 nm). The nominal thickness of Mo spacer layer was varied from 0 to 1 nm. The Mo (20 nm) underlayer and SiN (30 nm) capping layer were deposited at room temperature. The substrate was pre-annealed at 700° C for 30 min after underlayer deposition and then the Nd-Fe-B (16 nm) layer was deposited at substrate temperature $T_s^{Nd\text{-}Fe\text{-}B} = 500$ °C to get a (0 0 1) crystallographic texture. The Nd-Fe-B thin film was post annealed at 550 °C for 1 h for improving the crystallinity and the texture. During the Nd-Fe-B layer deposition, the Ar gas pressure was fixed at 0.17 Pa with sputtering powers for Nd (99.9 at.%) target at 14 W, for Fe (99.99 at.%) target at 8 W and for $Fe_{80}B_{20}$ target at 76 W. The spacer Mo (d_{Mo} nm) and $Ni_{80}Fe_{20}$ (5 nm) layers were deposited on top of Nd-Fe-B layer at room temperature. A single layer Nd-Fe-B with the form of MgO (1 0 0) sub./Mo (20 nm)/Nd-Fe-B (16 nm)/Mo (20 nm) and a single layer $Ni_{80}Fe_{20}$ film with the form of thermally oxidized Si sub./Ta (20 nm)/$Ni_{80}Fe_{20}$ (5 nm)/Ta (20 nm) were also fabricated as a reference sample. All of these samples were prepared at the same chamber base pressure but deposition time varied with the thickness of thin film layer. A slightly thicker capping layer was chosen for all the samples in order to prevent oxidation and degradation of the film with time and during exposure to a high-power femtosecond laser during the time-resolved measurements in air. We label these samples as S1–S3 and their stacking structure are as following:

S1: MgO sub./Mo (20 nm)/Nd-Fe-B (16 nm)/Mo (20 nm),

S2: MgO sub./Mo (20 nm)/Nd-Fe-B (16 nm)/$Ni_{80}Fe_{20}$ (5 nm)/SiN (30 nm),

S3: MgO sub./Mo (20 nm)/Nd-Fe-B (16 nm)/Mo (1 nm)/$Ni_{80}Fe_{20}$ (5 nm)/SiN (30 nm),

The crystalline structure and microstructure were characterized by X-ray diffraction (XRD) and transmission electron microscopy (TEM) with energy dispersive spectroscopic (EDS) analysis. The static magnetic hysteresis loops at room temperature were measured using a superconducting quantum interference device (SQUID) magnetometer with in-plane and out-of-plane applied magnetic field up to ± 6 T. The ultrafast magnetization dynamics were measured by a TRMOKE microscope [20] in a two-color pump-probe scheme. An output of a Ti-sapphire regenerative amplifier with a wavelength of 800 nm, a pulse width of 200 fs, and a pulse repetition rate of 10 kHz was used as a probe, whereas its second harmonic at wavelength of 400 nm was used as a pump. The pump beam was chopped at 900 Hz with a mechanical chopper for a lock-in detection. The fluences of the pump and probe beams were 2 and 0.15 mJ/cm^2. The magneto-optical Kerr rotation of the probe beam after reflection from the sample was measured using a pair of balanced photodetectors as a function of the time delay between the pump and probe pulses. An external bias magnetic field ($\mu_0 H_b$) was applied at an angle of $\theta_H = 70°$ with respect to the perpendicular direction of the sample surface. The strength of the applied magnetic field can go up to 2 T.

3. Results and discussions

3.1. Magnetic properties and microstructures

Fig. 1(a) shows the XRD pattern of the S1–S3 films. A (0 0 4) peak of $Nd_2Fe_{14}B$ phase is observed for all the samples in addition to the substrate MgO (2 0 0) and Mo (2 0 0) peaks, which indicates that the $Nd_2Fe_{14}B$ has (0 0 1) texture. A peak around $2\theta = 31°$ corresponds to Nd-rich phase and another peak around $2\theta = 34°$ indicates the Nd_5Fe_{17} phase for all three samples. Fig. 1((b)–(d)) compare the perpendicular and in-plane magnetization curves of S1–S3 films. All the samples show the strong perpendicular anisotropy because of the c-axis texture of the samples. In the case of S1 film (Fig. 1(b)), a good squareness with B_r of 1.06 MA/m and $\mu_0 H_c$ of 2 T are observed in the perpendicular magnetization curve. However, in the in-plane magnetization curve, although the XRD patterns show the (0 0 1) texture, there is a large in-plane hysteresis ($\mu_0 H_c = 1.65$ T) which is due to misaligned $Nd_2Fe_{14}B$ grains. By the deposition of $Ni_{80}Fe_{20}$ layer on the Nd-Fe-B layer (S2) (Fig. 1(c)), $\mu_0 H_c$ of easy axis reduces to 1.28 T. Due to the strong exchange coupling between Nd-Fe-B and $Ni_{80}Fe_{20}$ layers, the magnetization curve behaves as a single phase magnet. The remanence magnetization B_r is about 0.92 MA/m which is smaller than that of S1 film because of small M_s in $Ni_{80}Fe_{20}$. In the in-plane magnetization curve, the soft magnetic behavior can be seen around zero field due to the magnetization reversal of the $Ni_{80}Fe_{20}$ layer. When 1 nm thick Mo spacer layer is introduced in between Nd-Fe-B and $Ni_{80}Fe_{20}$ layers (S3) (Fig. 1(d)), $\mu_0 H_c$ of easy axis recovered to 1.9 T. In the perpendicular direction, the magnetization gradually decreases in second quadrant same as S2 film. However, a step like behavior is observed due to the decoupling of the exchange between the Nd-Fe-B and $Ni_{80}Fe_{20}$ layers.

In order to understand these magnetization behaviors, we observed the microstructures for S1–S3 samples. Fig. 2 shows the STEM-HAADF images [(a), (c), (e)] and corresponding EDS maps [(b), (d), (f), (g)] for the samples of S1–S3. From the cross-sectional STEM-HAADF images, it can be observed that the interface between each layer is quite sharp and well separated. The surface of the Nd-Fe-B layer is found to be little rough because of the high deposition temperature. The EDS analysis shows there is no notable inter-diffusion of materials between each layer and there are Nd-rich regions as shown by the arrows in Fig. 2(b). In the case of S3, although the thickness of Mo spacer layer is only 1 nm,

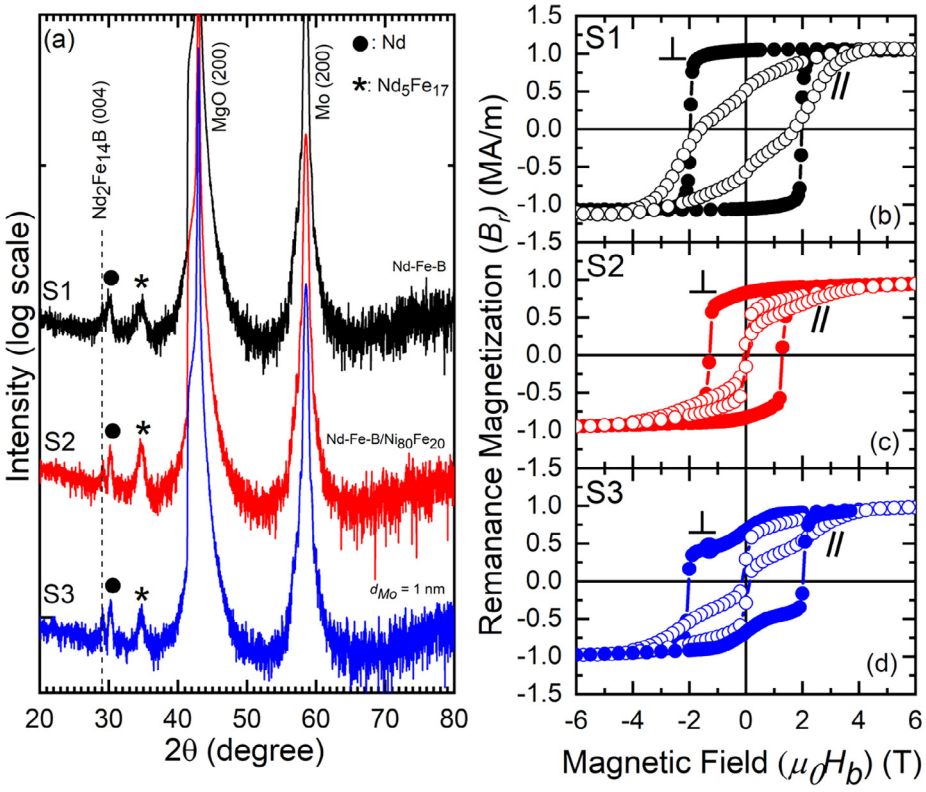

Fig. 1. (a) X-ray diffraction patterns for S1–S3 films. (b–d) Magnetization curves (filled and open circles corresponds to out-of-plane and in-plane direction respectively) for (b) S1, (c) S2, and (d) S3 films.

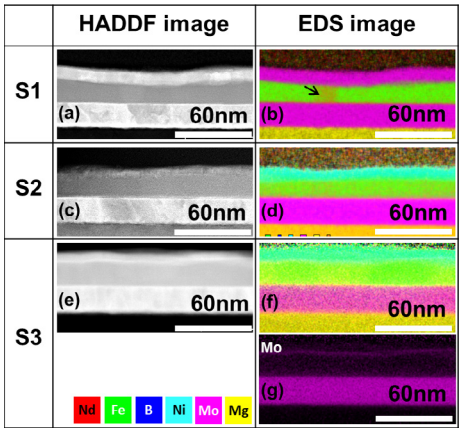

Fig. 2. STEM-HAADF images [(a), (c), (e)] and corresponding EDS maps [(b), (d), (f), (g)] for the samples of S1–S3.

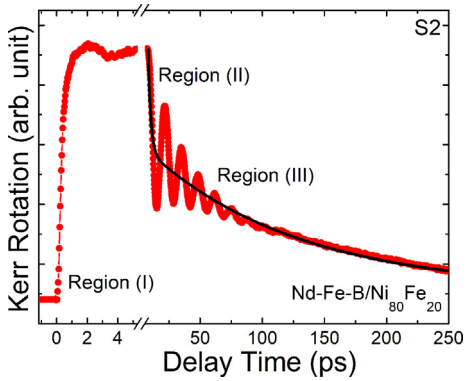

Fig. 3. Typical time-resolved Kerr signal for S2 film at $\mu_0 H_b = 2$ T showing three different temporal regions (I, II, and III).

we can find Mo layer (Fig. 2(g)) clearly in Mo EDS map and there is no diffusion of Mo element either in Nd-Fe-B or in $Ni_{80}Fe_{20}$ layers. Therefore, the step-like behavior in the S3 sample is thought to be due to the decoupling of the two ferromagnetic layers by 1 nm thick Mo layer.

3.2. Magnetization dynamics

In order to evaluate the interlayer exchange coupling between the Nd-Fe-B and $Ni_{80}Fe_{20}$ layers, we studied the time-resolved magnetization dynamics using TRMOKE microscope [20]. Fig. 3 shows the representative experimental results of time-resolved magneto-optical Kerr rotation for S2 film at $\mu_0 H_b = 2$ T. The time-domain oscillatory signal consists of three different temporal regions. Region (I) corresponds to ultrafast demagnetization (~500 fs) due to the incoherent interaction [21] in between electron and spin of the ferromagnetic thin film. The region (II) and (III) mainly denotes fast re-magnetization (t_1) because of the relaxation of energies of electron and spin to the lattice [22] and slow re-magnetization (t_2) due to relaxation of energy from the lattice to the substrate and surroundings followed by oscillatory precessional motion. In case of S2 thin film, the value of t_1 and t_2 is 2 ps and 121 ps, respectively. Resonance frequency (f_r) of the time-domain oscillatory signal can be derived by performing Fast-Fourier transform (FFT) of the bi-exponential back-ground subtracted time-resolved Kerr signal. Since the resonance frequency of Nd-Fe-B is high due to the high magnetic anisotropy, it is hard to detect the signal from single layer Nd-Fe-B thin films using FMR experiment [16,17]. On the other hand, using TRMOKE microscope, we successfully probe the magnetization dynamics of the Nd-Fe-B (16 nm) film (S1). Fig. 4(a) shows the raw time-resolved Kerr rotation data and the corresponding FFT spectra (Fig. 4(b)) for S1–S3 films at the bias field ($\mu_0 H_b$) = 2 T. For the S1 film, we found two different resonance frequency modes (mode 1 and 2). The

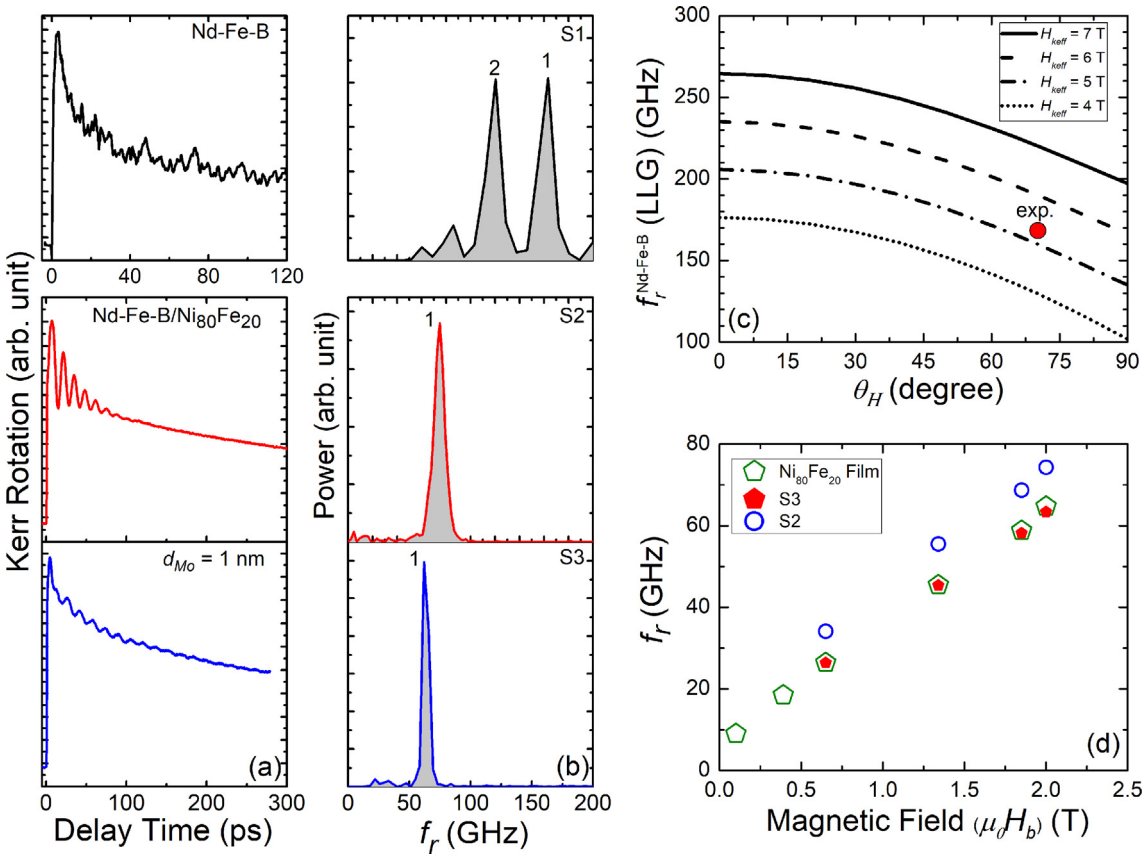

Fig. 4. (a) Measured raw time-resolved Kerr rotations data and (b) corresponding FFT spectra are shown for S1–S3 films at $\mu_o H_b = 2$ T. (c) Resonance frequency (f_r) calculated using the linearized LLG equation at various effective anisotropy field H_{keff} plotted as a function of bias magnetic field angle θ_H for Nd-Fe-B (16 nm) thin film. (d) Comparison of resonance frequency (f_r) measured for $Ni_{80}Fe_{20}$ (5 nm) thin film, S2 and S3 film at various strength of bias magnetic field for $\theta_H = 70^\circ$.

value of mode 1 is 161 GHz and that of mode 2 is 119 GHz. we calculate the resonance frequency (f_r) using the linearized LLG equation at various effective anisotropy field H_{keff} as a function of bias magnetic field angle θ_H for Nd-Fe-B (16 nm) thin film (Fig. 4(c)). The spin precession frequency is generally derived from a linearized Landau-Lifshitz-Gilbert (LLG) equation [23,24]:

$$f_r = \frac{\gamma}{2\pi}\sqrt{H_1 H_2} \tag{1}$$

where γ is the gyromagnetic ratio. H_1 and H_2 are given by:

$$H_1 = H_b\cos(\theta_H - \theta_1) + H_{keff}\cos^2\theta_1 \tag{2}$$

$$H_2 = H_b\cos(\theta_H - \theta_1) + H_{keff}\cos 2\theta_1 \tag{3}$$

with θ_H and θ_1 being the angles of H_b and the magnetization in the Nd-Fe-B film with respect to the perpendicular direction of the film surface, and H_{keff} is an effective anisotropy field. The equilibrium angle of the magnetization is determined by,

$$\sin 2\theta_1 = \left(\frac{2H_b}{H_{keff}}\right)\sin(\theta_1 - \theta_H) \tag{4}$$

The red dot in Fig. 4(c) shows the experimental data at $\theta_H = 70^\circ$ for $\mu_o H_b = 2$ T considering the $H_{keff} = 5$ T (measured from magnetization curve). So the theoretical calculation indicates that the origin of mode 1 of S1 film is due to the total effective magnetic field of highly anisotropic Nd-Fe-B thin film. The origin of mode 2 is not clear at present and requires further analysis. In the case of S2 bilayer thin film, a remarkable difference is observed in the TRMOKE spectra. It shows single resonance frequency mode (mode 1) instead of two resonance frequency modes and the value drastically reduces to 74.4 GHz. In the case of the S3 film, we observe single frequency mode again and the value of mode 1 further reduces to 63.4 GHz respectively. Observation of single resonance frequency mode and their reduced value indicate that the magnetization dynamics is basically governed by the top $Ni_{80}Fe_{20}$ layer for the bilayer (S2) and spacer layer inserted samples (S3). For comparison, we studied the magnetization dynamics of the reference $Ni_{80}Fe_{20}$ thin film and found that the resonance frequency value (Fig. 4(d)) of single layer $Ni_{80}Fe_{20}$ film is less compared to the resonance frequency of the S2 film. However, the value is quite comparable with the resonance frequency of the S3 film. For the S2 thin film, the total effective magnetic field is higher compared to the S3 film as the top $Ni_{80}Fe_{20}$ layer feels the large anisotropic field contribution due to strong interlayer exchange coupling between the Nd-Fe-B and $Ni_{80}Fe_{20}$ layers. In the case of S3 film, the interlayer exchange coupling decreases due to the presence of the Mo spacer layer which reduces the anisotropic field contribution from the Nd-Fe-B layer and as a result the total effective magnetic field of the top $Ni_{80}Fe_{20}$ layer reduces. So, the resonance frequency behavior of the S3 film is comparable with the single layer $Ni_{80}Fe_{20}$ thin film.

In order to quantify the interlayer exchange coupling constant, a simplified model calculation for the bilayer model (hard/soft) as shown in the inset of Fig. 5 is proposed. This calculation is based on the macrospin (single-domain) model which approximates the uniform magnetization precession in each magnetic layer. The total energy per unit area is expressed as follows;

$$E(\theta_1, \theta_2) = -d_1 M_s^1 H_b\cos(\theta_1 - \theta_H) - d_1 K_{u,eff}^1\cos^2\theta_1 - d_2 M_s^2 H_b\cos(\theta_2 - \theta_H) - d_2 K_{u,eff}^2\cos^2\theta_2 - 2J_{ex}\cos(\theta_1 - \theta_2) \tag{5}$$

where d_i is the thickness of the film ($i = 1$ for Nd-Fe-B and $i = 2$ for $Ni_{80}Fe_{20}$), M_s^i is the saturation magnetization, $K_{u,eff}^i$ is the anisotropy constant of each magnetic layer and J_{ex} is the interlayer exchange

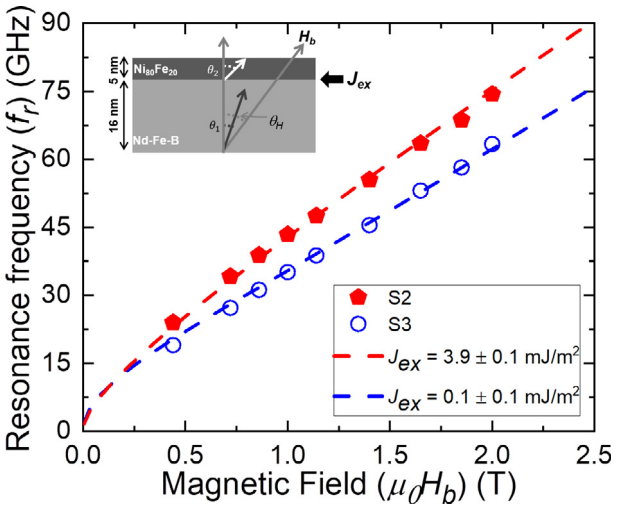

Fig. 5. Experimental (points) and calculated (dotted curves) resonance frequencies are shown for different thickness (d_{Mo}) of Mo (S2 and S3) as a function of $\mu_0 H_b$. Value of exchange-coupling constant J_{ex} is expressed in units of mJ/m^2. Schematic representation and definition of angle of magnetization and applied external bias field in the bilayer structure of the sample is shown in inset.

coupling constant. θ_H, θ_i are the angles of the external applied magnetic field ($\mu_0 H_b$) and magnetic moment in each layer with respect to the normalized direction of the film plane respectively. In the total energy expression, the 1st and 3rd terms correspond to Zeeman energies, 2nd and 4th terms are the anisotropy energies of the Nd-Fe-B layer and Ni$_{80}$Fe$_{20}$ layers respectively. The 5th term represents the interlayer exchange-coupling energy. When this bilayer system is located in an applied static magnetic field, the magnetic moment will precess around its equilibrium direction which can be expressed by following equation;

$$\frac{1}{\gamma}\frac{d\boldsymbol{M}_i}{dt} = -\frac{1}{d_i}\frac{\boldsymbol{M}_i}{M_s^i} \times \nabla_i E(\theta_1, \theta_2) \tag{6}$$

where $\boldsymbol{M}_i$ is the magnetization vector in each layer. If the time variation of $\boldsymbol{M}_i$ depend on $e^{-i\omega t}$ form, where the $\omega(=2\pi f_r)$ is the angular frequency, the matrix form can be obtained as described in the literature of Zhang et al. [25]. The determinant of the 4 × 4 matrix will give the following relationship between the angular resonance frequency and the external bias magnetic field.

$$\omega^4 + b\omega^2 + c = 0 \tag{7}$$

where

$$b = \frac{E_{\theta_1\theta_1}E_{\varphi_1\varphi_1}}{(d_1 M_s^1/\gamma_1 \sin\theta_1)^2} + \frac{E_{\theta_2\theta_2}E_{\varphi_2\varphi_2}}{(d_2 M_s^2/\gamma_2 \sin\theta_2)^2} + \frac{E_{\theta_1\theta_2}E_{\varphi_1\varphi_2}}{(d_1 M_s^1/\gamma_1 \sin\theta_1)(d_2 M_s^2/\gamma_2 \sin\theta_2)}$$

$$c = \frac{E_{\theta_1\theta_2}E_{\varphi_1\varphi_2}}{(d_1 M_s^1/\gamma_1 \sin\theta_1)^2 (d_2 M_s^2/\gamma_2 \sin\theta_2)^2}\left((E_{\theta_1\theta_2}E_{\varphi_1\varphi_2})^2 - (E_{\theta_1\theta_2})^2 E_{\varphi_1\varphi_1}E_{\varphi_2\varphi_2} - (E_{\varphi_1\varphi_2})^2 E_{\theta_1\theta_1}E_{\theta_2\theta_2} - (E_{\theta_1\theta_1}E_{\varphi_1\varphi_1})(E_{\theta_2\theta_2}E_{\varphi_2\varphi_2})\right)$$

Here,

$$E_{\theta_i\theta_j} = \frac{\partial^2 E(\theta_1, \theta_2)}{\partial\theta_i \partial\theta_j},\ E_{\varphi_i\varphi_j} = \frac{\partial^2 E(\theta_1, \theta_2)}{\partial\varphi_i \partial\varphi_j}(\varphi_i = \varphi_j)(i, j = 1 \text{ or } 2)$$

where φ is the angle of magnetization in each layer in the in-plane direction. Fig. 5 shows the calculated and measured resonance frequency (f_r) plotted as a function of the strength of the external bias magnetic field ($\mu_0 H_b$) at a fixed θ_H. f_r increases with the magnetic field in all the samples. By the Mo insertion, the slope of the magnetic field dependence line decreases. The broken dotted line shows the fitting results whereas the dot shows the experimental values of the resonance frequency. We found that the degree of fitting between the calculated and the measured data are quite satisfactory and the used parameters

Table 1
Material parameter values of Nd-Fe-B and Ni$_{80}$Fe$_{20}$ film for calculation of f_r *vs.* $\mu_0 H_b$using macrospin modeling.

Material	Nd-Fe-B	Ni$_{80}$Fe$_{20}$
g	2.1	2.1
M_s (MA/m)	1.06	0.86
$K_{u,eff}$ (J/m^3)	3.4 × 10^6	0

for the calculation are shown in Table 1.

The calculated f_r with J_{ex} = 3.9 ± 0.1 mJ/m^2 well reproduces the experimental data points over whole bias field range for the Nd-Fe-B/Ni$_{80}$Fe$_{20}$ bilayer film (S2) as shown in Fig. 4. This good agreement between the theoretical and experimental data implies that the growth of soft magnetic layer on top of hard magnetic layer has a nice interface and both are coupled with strong exchange coupling. In the case of the S3 film, we also found a good agreement between the theoretical and experimental data points of f_r, and fitting deduced the value of J_{ex} = 0.1 ± 0.1 mJ/m^2. So this result implies that the presence of Mo spacer layer in between Nd-Fe-B/Ni$_{80}$Fe$_{20}$ magnetic layers almost decouple the strong exchange coupling between them. It should be noted that for d_{Mo} = 1 nm (S3) the $\mu_0 H_c$ value recovers, a kink is formed in the demagnetization curve and the resonance frequency significantly reduces compared with the coupled bilayer thin film (S2) which implies the decoupling of the exchange coupled system. Later on we estimated the value of J_{ex} for thicker (3 nm) Mo insertion layer and observe the similar results as for 1 nm Mo thick layer. So we can conclude that 1–3 nm thick Mo insertion layer is sufficient to decouple the strong exchange coupling between Nd-Fe-B and Ni$_{80}$Fe$_{20}$ layer. In previous study, Kato et al. [15] reported the value of J_{ex} = 4 mJ/m^2 for Nd-Fe-B nanocomposite magnet containing α-Fe. So, our evaluated value of J_{ex} is comparable with previous reported results [16,17].

In order to verify the J_{ex} value estimated from TRMOKE and macrospin modeling, we carried out a micromagnetic calculation [15,26] of magnetization curve. A system of 5 × 5 × 6 rectangular parallelepiped cells are assumed, in which bottom 5-layer cells are hard phase and top 1-layer cell is soft phase. The cell size was set to 10 nm along *x*, *y* directions, and 3.2 nm and 5 nm along *z* direction in hard and soft phase, respectively. The total energy E of the system is assumed to be expressed by

$$E = E_J + E_K + E_D + E_{ext} \tag{8}$$

where E_J, E_K, E_D, and E_{ext} denotes the exchange energy between neighboring grains, anisotropy energy of each grain, demagnetizing energy, and Zeeman energy, respectively. We used the values of saturation magnetization M_s for Nd-Fe-B and Ni$_{80}$Fe$_{20}$ described in Table 1. We set the uniaxial anisotropy constants $K_{u,eff}^{Nd-Fe-B} = 2 \times 10^6$ J/m^3 so as to best fit the observed coercivity, because a simplified model as given here often leads to a serious overestimate of coercivity by using actual anisotropy value described in Table 1, and for$K_{u,eff}^{Ni_{80}Fe_{20}} = 0$. Fig. 6 shows the calculated magnetization curve without exchange coupling (J_{ex} = 0) (Fig. 6(b)) and with the J_{ex} of 3.9 mJ/m^2 (Fig. 6(a)) which was estimated from TRMOKE. These are well reproduced the experimental magnetization curve for without (S3) and with (S2) exchange coupling. So the J_{ex} of 3.9 mJ/m^2 estimated from TRMOKE is adequate value in terms of magnetization curves.

To discuss about the origin of this interlayer exchange coupling, we may think about many different types of coupling mechanism such as famous RKKY type coupling or quantum well model *etc*. These types of couplings are basically based on the conduction electrons that mean the interface of interlayer should be atomically flat. But in our case the interface between each layer is not atomically flat so those above mentioned coupling mechanism may not play an important role. As well as due to the atomically rough interface the dipolar coupling in the interface may overcome the conduction electrons based coupling. Therefore, it is difficult to explain the exact origin of the coupling

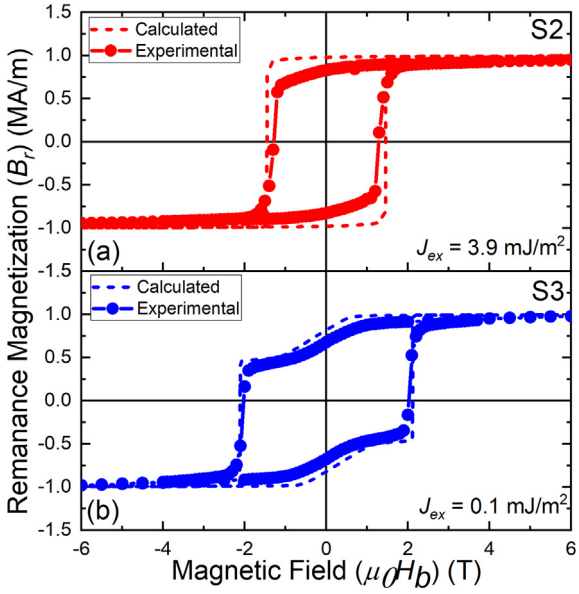

Fig. 6. Calculated Magnetization curves using micromagnetic simulation for S2 (a) and S3 (b) films in comparison with the measured magnetization curves by SQUID-VSM. The value of exchange coupling constant J_{ex} for micromagnetic simulation is shown in the graph (a, b) in the unit of mJ/m^2.

mechanism in our case.

4. Conclusion

In summary, we have systematically investigated the interlayer exchange coupling constant in Nd-Fe-B (16 nm)/Mo (d_{Mo} nm)/$Ni_{80}Fe_{20}$ (5 nm) multilayer thin film. We have excited and detected the magnetization dynamics of this film structures by the all-optical TRMOKE microscope. $\mu_0 H_c$ decreases to 1.28 T in the Nd-Fe-B/$Ni_{80}Fe_{20}$ film vis-à-vis $\mu_0 H_c$ = 2 T for Nd-Fe-B single layer thin film. However, it recovers to 1.9 T by the insertion of Mo layer in between the Nd-Fe-B and $Ni_{80}Fe_{20}$ magnetic layers. Microstructure shows a clear interface and no inter-diffusion of elements between the layers. The dynamics show two clear high frequency resonance modes at the saturation magnetic field for the single layer Nd-Fe-B film. We found that the magnetization dynamics of $Ni_{80}Fe_{20}$ on Nd-Fe-B strongly depends on the interlayer exchange coupling and high anisotropy field of hard magnetic thin film. By performing TRMOKE, macro spin modeling and micromagnetic simulations we confirmed that the exchange coupling between the Nd-Fe-B and $Ni_{80}Fe_{20}$ layers in the Nd-Fe-B/$Ni_{80}Fe_{20}$ film is J_{ex} = 3.9 ± 0.1 mJ/m^2. For Nd-Fe-B/Mo/$Ni_{80}Fe_{20}$ sample, we find the value of J_{ex} = 0.1 ± 0.1 mJ/m^2, more than one order of magnitude smaller than that for the directly coupled film. So the existence of spacer layer decouples the exchange coupled system. We established the estimation method of the interlayer exchange coupling constant in the hard/soft magnetic bilayer film system. It would be possible to apply this method to the intergranular exchange coupling system such as exchange-coupled conventional Nd-Fe-B magnets and also the diffusion processed Nd-Fe-B magnet to estimate the intergranular exchange coupling quantitatively.

Acknowledgement

This work was supported by Elements Strategy Initiative Center for Magnetic Materials (ESICMM), an outsourcing project of the Ministry of Education, Culture, Sports, Science and Technology, Japan.

References

[1] R. Coehoorn, D.B. de Mooij, C. de Waard, J. Magn. Magn. Mater. 80 (1989) 101–104.
[2] E.F. Kneller, R. Hawig, IEEE Trans Magn. 27 (1991) 3588–13560.
[3] R. Skomski, J.M.D. Coey, Phys. Rev. B 48 (1993) 15812–15816.
[4] T. Schrefl, H. Kronmüller, J. Fidler, J. Magn. Magn. Mater. 127 (1993) L273–L277.
[5] I.A. Al-Omari, D.J. Sellmyer, Phys. Rev. B 52 (1995) 3441–3447.
[6] S.M. Parhofer, J. Wecker, C. Kuhrt, G. Gieres, L. Schultz, IEEE Trans Magn. 32 (1996) 4437–4439.
[7] J. Zhang, Y.K. Takahashi, R. Gopalan, K. Hono, Appl. Phys. Lett. 86 (2005) 122509.
[8] H. Fukunaga, H. Nakamura, Scripta Mater. 44 (2001) 1341–1345.
[9] M. Shindo, M. Ishizone, A. Sakuma, H. Kato, T. Miyazaki, J. Appl. Phys. 81 (1997) 4444–4446.
[10] H. Kato, M. Ishizone, K. Koyama, T. Miyazaki, J. Magn. Magn. Mater. 290 (2005) 1221–1225.
[11] W.B. Cui, W. Liu, J. Li, F. Yang, Q. Zhang, X.G. Liu, Z.D. Zhang, J. Phys. D: Appl. Phys. 41 (2008) 245007.
[12] W.B. Cui, W. Liu, W.J. Gong, X.H. Liu, S. Guo, F. Yang, Z.H. Wang, Z.D. Zhang, J. Appl. Phys. 111 (2012) 07B503.
[13] W.B. Cui, S.J. Zheng, W. Liu, X.L. Ma, F. Yang, Q. Yao, X.G. Zhao, Z.D. Zhang, J. Appl. Phys. 104 (2008) 053903.
[14] W.B. Cui, Y.K. Takahashi, K. Hono, Adv. Mater. 24 (2012) 6530–6535.
[15] H. Kato, M. Ishizone, T. Miyazaki, K. Koyama, H. Nojiri, M. Motokawa, IEEE Trans. Magn. 37 (2001) 2567–2569.
[16] D. Ogawa, K. Koike, H. Kato, S. Mizukami, T. Miyazaki, M. Oogane, Y. Ando, J. Kor. Phys. Soc. 63 (2013) 489–492.
[17] D. Ogawa, K. Koike, S. Mizukami, T. Miyazaki, M. Oogane, Y. Ando, H. Kato, Appl. Phys. Lett. 107 (2015) 102406.
[18] L.R. Shelford, Y. Liu, U. Al-Jarah, P.A.J. de Groot, G.J. Bowden, R.C.C. Ward, R.J. Hicken, Phys. Rev. Lett. 113 (2014) 067601.
[19] S. Pal, S. Barman, O. Hellwig, A. Barman, J. Appl. Phys. 115 (2014) 17D105.
[20] Y.K. Takahashi, Y. Miura, R. Choi, T. Ohkubo, Z.C. Wen, K. Ishioka, R. Mandal, R. Medapalli, H. Sukegawa, S. Mitani, E.E. Fullerton, K. Hono, Appl. Phys. Lett. 110 (2017) 252409.
[21] E. Beaurepaire, J.C. Merle, A. Daunois, J.Y. Bigot, Phys. Rev. Lett. 76 (1996) 4250–4253.
[22] A. Laraoui, J. Vénuat, V. Halté, M. Albrecht, E. Beaurepaire, J.-Y. Bigot, J. Appl. Phys. 101 (2007) 09C105.
[23] S. Mizukami, F. Wu, A. Sakuma, J. Walowski, D. Watanabe, T. Kubota, X. Zhang, H. Naganuma, M. Oogane, Y. Ando, T. Miyazaki, Phys. Rev. Lett. 106 (2011) 117201.
[24] M. Shigemi, A. Hiroyuki, W. Daisuke, O. Mikihiko, A. Yasuo, M. Terunobu, Appl. Phys. Exp. 1 (2008) 121301.
[25] Z. Zhang, L. Zhou, P.E. Wigen, K. Ounadjela, Phys. Rev. B 50 (1994) 6094–6112.
[26] M. Ishizone, T. Nomura, H. Kato, T. Miyazaki, M. Motokawa, J. Magn. Soc. Jpn. 24 (2000) 423–426.